Equivalent-circuit Models of Grid-forming IBRs for Electromagnetic-transient Simulations

Nathan Baeckeland*, Thomas Ankner*, Sairaj Dhople†, Brian B. Johnson‡, and Gab-Su Seo*

*Power Systems Engineering Center, National Renewable Energy Laboratory, Golden, CO, USA
†Department of Electrical and Computer Engineering, University of Minnesota, Minneapolis, MN, USA
‡Chandra Family Department of Electrical and Computer Engineering, University of Texas, Austin, TX, USA
E-mails: {nathan.baeckeland, thomas.ankner, gabsu.seo}@nrel.gov, sdhople@umn.edu, b.johnson@utexas.edu

***Abstract*—We derive equivalent-circuit models of control- and physical-layer subsystems of grid-forming (GFM) inverter-based resources (IBRs) for electromagnetic-transient (EMT) simulations. Three different primary controllers are considered: Droop, Virtual Synchronous Machine (VSM), and dispatchable Virtual Oscillator Control (dVOC). In addition, the models include cascaded voltage- and current-control loops, and LCL output filters. Simulations for a single-inverter setup and for a network of five inverters in a modified IEEE 14-bus topology are presented. The equivalent-circuit models simulated with analog electronic circuit-simulator software (in our case, LTspice) offer the same accuracy with up to $150\times$ lower computational burden compared to block-diagram-based implementations in commercial off-the-shelf EMT software (in our case, MATLAB-Simulink).**

***Index Terms*—Electromagnetic transient simulation, equivalent-circuit models, grid-forming inverters.**

I. Introduction

Electromagnetic transient (EMT) domain simulations are becoming increasingly commonplace for controller tuning and dynamic-security assessment of power grids featuring inverter-interfaced renewable energy resources [1]. Concurrently, grid-forming (GFM) inverter-based resources (IBRs) are widely recognized as enabling technologies to address a wide range of frequency- and voltage-related challenges across scales [2]. Therefore, there is a critical need to develop computational machinery that can facilitate lean and accurate EMT simulations of grids featuring GFM IBRs. Taking a step in this direction, this paper puts forth equivalent-circuit models of control- and physical-layer subsystems of GFM IBRs. This is pursued with the deliberate intent of building network-level EMT simulations featuring equivalent-circuit models in analog electronic circuit-simulator software that are widely celebrated for their scalability (since they are used to simulate integrated circuits that feature significant complexity).

Using equivalent analog circuits to represent the behavior of electromechanical and electromagnetic devices has been common practice in classical power theory [3]. Equivalent-circuit representations for physical-layer dynamics of power converters are also commonplace [4]–[6]. More recently, these efforts have been expanded to include IBRs. In [7], equivalent-circuit models for control- and physical-layer dynamics of current-controlled inverters were presented. These were extended to include several distinguishing attributes of grid-following IBRs in [8]. In [9], analog electronic simulation software was used to implement EMT simulations of grid-following IBR models for networks scaling up to 118 buses. Building on these prior works—which only address grid-following inverter controls—we present equivalent-circuit models in the positive sequence for grid-forming IBRs. Three representative GFM primary controls are modeled in an integrated common platform in this work: Droop, Virtual Synchronous Machine (VSM), and dispatchable Virtual Oscillator Control (dVOC). (See, e.g., [10]–[12] for efforts that pursue integrated modeling of GFMs.) We validate and compare these models through single-inverter and network-scale simulations. The baseline is established by block-diagram commercial off-the-shelf EMT software (MATLAB-Simulink), and the equivalent-circuit models are developed in LTspice (a popular analog electronic circuit-simulator software). The results illustrate that simulations in LTspice can yield a decrease in the computational time of approximately $150\times$ with no discernible loss in accuracy.

The remainder of the paper is structured as follows. In Section II, we illustrate how control blocks can be cast into circuits, and we derive an equivalent-circuit schematic for a GFM inverter. In Section III, we validate the circuit representation through single-inverter simulations and a 14-bus network simulation. Finally, we conclude in Section IV.

II. Equivalent-circuit Representation of GFM IBRs

In this section, we explain how control blocks can be translated into equivalent circuits comprising interconnected passive RLC elements, varistors, and voltage/current-dependent voltage/current sources. Building on this, we present the corresponding equivalent-circuit model for a prototypical GFM IBR system comprising an LCL output filter, primary controller, voltage controller, current controller, and reference-frame transformations.

A. Overview of Equivalent-circuit Representation

Figure 1 illustrates how several computational and control operations germane to a variety of IBR control architectures—including addition, multiplication, integration, proportional-integral (PI) control, and projection in the Euclidean space—

can be realized with passive RLC elements, varistors, and voltage-/current-dependent voltage/current sources.

Addition is accomplished by paralleling two current sources or placing two voltage sources in series; see Fig. 1(a). Since multiplication is a nonlinear operation, varistors in conjunction with current/voltage sources are utilized to realize it. Notice that both realizations for multiplication illustrated in Fig. 1(b) do not preserve consistency of the units of measurement. For instance, a signal resulting from a voltage measurement (bearing units of Volts) can feature as an input for the varistor (bearing units of Ohms); however, this is not unreasonable since these circuits are not physical systems but only a means to simulate control realizations. Integration, illustrated in Fig. 1(c), can be realized with an inductance or capacitor. The initial conditions of the inductor current or capacitor voltage should match the initial condition of the integrator state; this is not explicitly depicted. A PI controller in the circuit domain can be realized with a parallel RL circuit or a series RC circuit; see Fig. 1(d). Finally, projection of vectors in different reference frames is a matrix operation that can be realized with current sources and varistors that are a function of the angular separation of the reference frames. In the remainder of this paper, we visualize projection via the shorthand four-port element illustrated in Fig. 1(e).

The same mathematical operation can be translated into equivalent circuits in different ways. In the realizations we put forth for addition, multiplication, integration, and PI control, note that one set uses voltage sources, and the other uses current sources. (Projection can be realized with voltage sources as well but with added complexity, and it is not presented here.) In the equivalent-circuit GFM IBR model discussed subsequently, we pick the circuit realization that preserves the unit of measurement to the extent possible (i.e., we strive for voltage measurements to feed into voltage sources, and current measurements to feed into current sources).

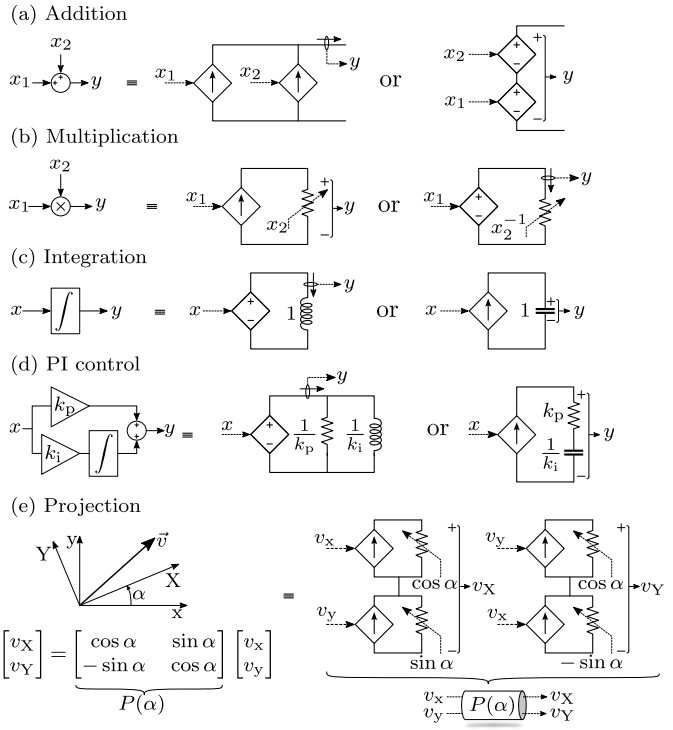

Fig. 1: Equivalent-circuit realization of (a) addition, (b) multiplication, (c) integration, (d) PI control, and (e) projection.

B. System Architecture of GFM IBRs realized with an Equivalent-circuit Representation

The generic control architecture and output-filter arrangement of a GFM IBR that is examined in this work is illustrated in Fig. 2(a). We consider a prototypical control flow with cascaded inner-current control, outer-voltage control, and primary control. Park's reference-frame transformations translate signals sensed in the abc reference frame to a local direct-quadrature (dq) reference frame. The primary control generates the reference voltage and frequency (and by extension, angle) based on sensed terminal signals (voltages and currents) and active- and reactive-power setpoints. The inner-current and outer-voltage control loops are PI controls with appropriate feed-forward terms that decouple the direct and quadrature signals to improve dynamic performance. Details about the control architecture are widely available in the literature, e.g., [13], [14]. With the aid of the dictionary established in Fig. 1, the GFM-IBR control architecture and output-filter arrangement are cast into an equivalent-circuit representation illustrated in Fig. 2. Notice that the RLC filter is represented in a global DQ frame; this is an implementation choice. In the network-level simulations that are presented subsequently, all LCL filters and interconnecting transmission lines are represented in a global DQ reference frame. The details of the circuit representation of the primary controllers, i.e., Droop, VSM, and dVOC, are discussed next.

1) Droop Control: The dynamics of the angle reference, θ, and voltage reference, $E^\star$, with Droop control are: [15]

$$\frac{\mathrm{d}\theta}{\mathrm{d}t} = \omega_0 + m_\mathrm{p}(P^\star - \overline{P}), \tag{1a}$$

$$E^\star = E_0 + m_\mathrm{q}(Q^\star - \overline{Q}), \tag{1b}$$

where ω_0 is the nominal grid frequency; m_p denotes the ω-P droop gain; $P^\star$ and $\overline{P}$ represent the active-power reference and the low-pass-filtered GFM active-power output; $E^\star$ denotes the reference voltage feeding into the voltage controller; E_0 denotes the nominal output voltage; m_q represents the V-Q droop gain; and $Q^\star$ and $\overline{Q}$ denote the reference and low-pass filtered output reactive power, respectively. The filtered active- and reactive-power measurements are obtained from the measured values, P, Q, with the aid of low-pass filters with cut-off frequency, ω_c. Translating (1a)–(1b) into equivalent circuits yields the circuit diagram shown in Fig. 2(c).

2) Virtual Synchronous Machine (VSM): The VSM primary controller emulates the dynamic behavior of a synchronous machine. The particular instance we model augments Droop control with synthetic inertia. The VSM dynamics are: [16]

$$M\frac{\mathrm{d}^2\theta}{\mathrm{d}t^2} = P^\star - P + \frac{1}{m_\mathrm{p}}(\omega_0 - \omega), \tag{2a}$$

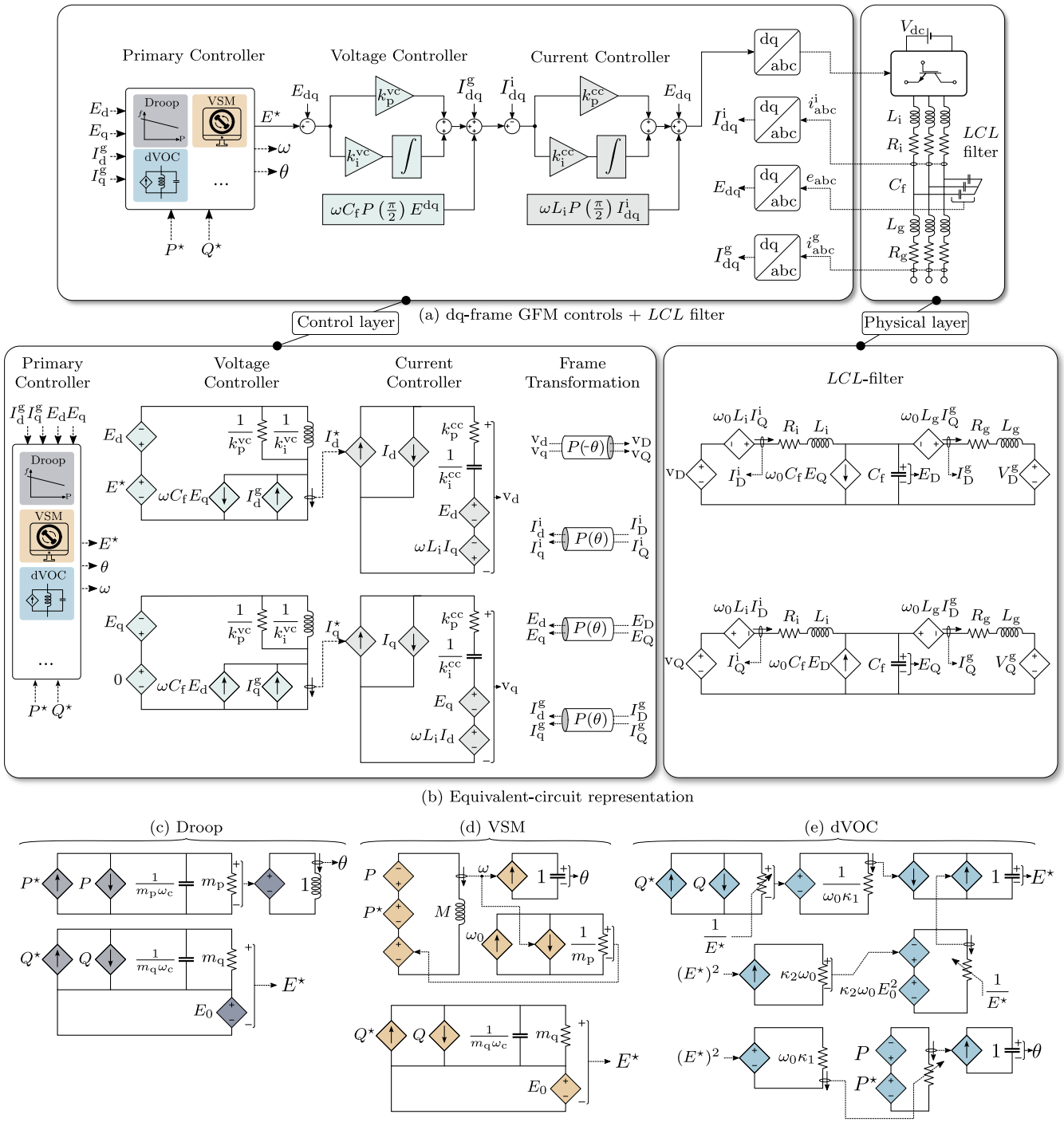

Fig. 2: (a) System-level dynamic model of GFM IBR (control- and physical-layer subsystems); (b) Corresponding equivalent-circuit representation with details on implementation of (c) Droop control, (d) Virtual Synchronous Machine (VSM) control, and (e) dispatchable Virtual Oscillator Control (dVOC).

$$E^\star = E_0 + m_\mathrm{q}(Q^\star - \overline{Q}), \tag{2b}$$

where M is an inertia constant. The circuit-domain translation of (2a)–(2b) is depicted in Fig. 2(d).

3) Dispatchable Virtual Oscillator Control (dVOC): This primary controller builds on the dynamics of the Andronov-Hopf oscillator. The governing dynamic equations are: [14]

$$\frac{\mathrm{d}\theta}{\mathrm{d}t} = \omega_0 + \frac{\kappa_1}{(E^\star)^2}(P^\star - P), \tag{3a}$$

$$\frac{\mathrm{d}E^\star}{\mathrm{d}t} = \kappa_2\omega_0 E^\star(E_0^2 - (E^\star)^2) + \frac{\kappa_2}{E^\star}(Q^\star - Q), \tag{3b}$$

where κ_1 and κ_2 denote the synchronization gain and voltage-amplitude gain of the controller, respectively. The circuit representation of (3a)–(3b) is shown in Fig. 2(e).

III. Validation via Numerical Simulations

In this section, we validate the equivalent-circuit GFM models for the three considered primary controllers through full-order EMT-domain simulations. Simulations for a single unit

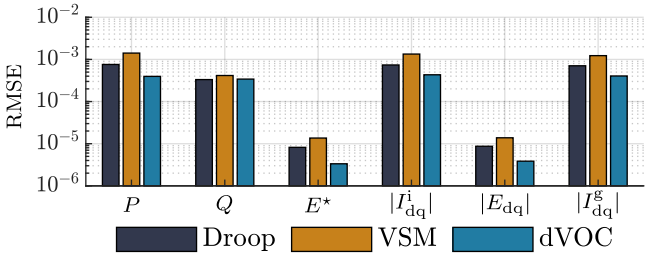

Fig. 3: Root-Mean-Square Errors (RMSE) between the block-diagram-based implementation in MATLAB-Simulink and the equivalent-circuit implementation in LTSpice for 6 signals.

and a modified IEEE 14-bus network are presented to benchmark the accuracy and computational effort of the equivalent-circuit representations. The equivalent-circuit models are set up in LTspice, whereas the conventional block-diagram-based models are built in MATLAB-Simulink. LTspice is an open-source analog electronic-circuit simulation software. It is not innately configured to simulate control-based actions (such as implementing PI controllers). As such, it is an ideal tool to validate the proposed circuit-based GFM models. No dedicated effort is expended in optimizing the simulation setups to minimize computation time in either LTspice or MATLAB-Simulink. Simulations are performed on a PC with an 11-th generation Intel Core i7-11800H processor and 32 GB of RAM. The model parameters are listed in Table I. All initial conditions are set to zero.

A. Single-unit Simulation

In this setup, we are interested in examining the accuracy of the equivalent-circuit modeling approach. The simulation involves a single GFM IBR with different primary controls connected to an infinite bus. A step change in the active-power setpoint, $P^\star$, from $0\,\mathrm{pu}$ to $0.5\,\mathrm{pu}$, and from $0.5\,\mathrm{pu}$ to $0.8\,\mathrm{pu}$, is implemented at $t{=}1\,\mathrm{s}$ and $t{=}2\,\mathrm{s}$, respectively. The setpoint for the reactive power remains at zero. Figure 3 illustrates the root-mean-square error (RMSE) between the simulations in MATLAB-Simulink and LTspice over the horizon $0.5\,\mathrm{s} < t < 2.5\,\mathrm{s}$. All primary-control types are considered, and errors are reported for 6 key signals. The results convey a near-perfect match between the two simulation approaches. Computational times for the two implementations are reported in Table II. Notice that the equivalent-circuit approach is approximately $100\times$ faster.

B. Network Simulation

In this section, we consider a modified IEEE 14-bus network with five GFM IBRs of different primary-control types. Figure 4 shows the network topology and indicates the types of primary controls used for each GFM IBR. The insets are meant to convey how the equivalent-circuit representations are modeled in LTspice. Line-impedance values are the same as those reported in [17]. We impose several setpoint command changes in active power. The reactive power setpoints remain at zero throughout. The simulation results are visualized in Fig. 5. The output active and reactive power of each GFM inverter is compared for the equivalent-circuit realization and the conventional block-diagram realization. The results convey a close match in waveforms. From the computational times reported in Table II, we note an approximately $150\times$ speedup with the equivalent-circuit realization.

TABLE I: Inverter and Network Parameters.

Parameter	Value	Unit	Parameter	Value	Unit
ω_0	$2\pi 60$	$\mathrm{rad}\cdot\mathrm{s}^{-1}$	$k_{\mathrm{p}}^{\mathrm{cc}}$	0.9817	pu
$\omega_0 L_{\mathrm{i}}$	0.0196	pu	$k_{\mathrm{i}}^{\mathrm{cc}}$	0.0018	pu
R_{i}	0.0139	pu	m_{p}	2	%
$\omega_0 C_{\mathrm{f}}$	0.1086	pu	m_{q}	5	%
$\omega_0 L_{\mathrm{g}}$	0.0196	pu	$k_{\mathrm{p}}^{\mathrm{vc}}$	1.4476	pu
R_{g}	0.0139	pu	$k_{\mathrm{i}}^{\mathrm{vc}}$	0.0273	pu
κ_1	0.0033	pu	M	0.0053	$\frac{\mathrm{s}^2}{\mathrm{rad}}$
κ_2	0.0796	pu			

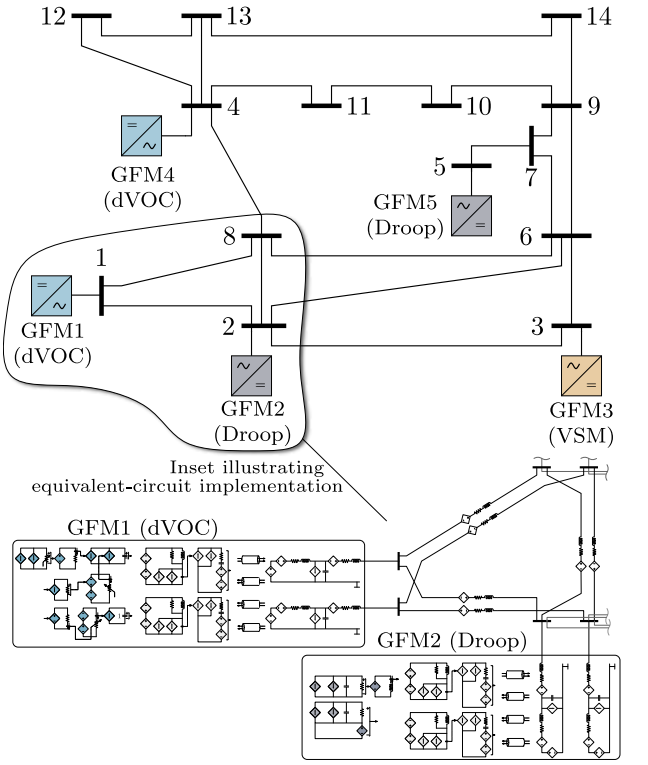

Fig. 4: Modified IEEE 14-bus network with five GFM IBRs of different primary-control types. Inset depicts how instances of the equivalent-circuit GFM IBR models from Fig. 2 are interfaced to the network.

TABLE II: Simulation run times for the equivalent-circuit realization in LTspice and the conventional block-diagram realization in MATLAB-Simulink.

Simulation type		MATLAB Simulink	LTspice
Single-unit	Droop	11.3 s	0.075 s
	VSM	11.6 s	0.070 s
	dVOC	12.1 s	0.062 s
Network		365 s	2.53 s

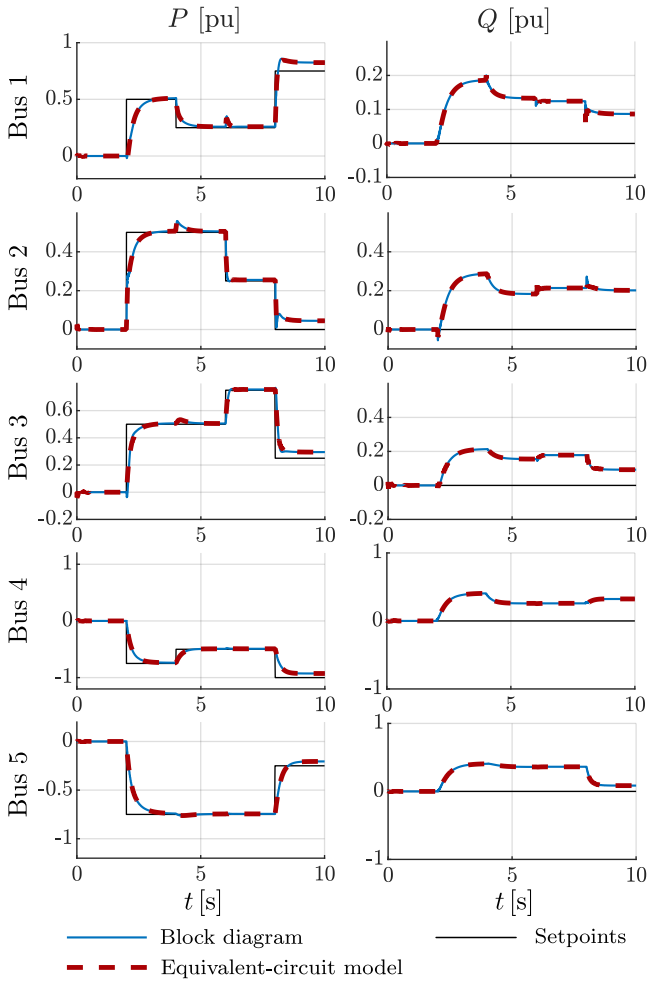

Fig. 5: Output active and reactive powers for all GFM IBRs in the modified IEEE 14-bus network illustrated alongside commanded references. Results from equivalent-circuit realization are superimposed to those from the conventional block-diagram realization.

IV. Concluding Remarks and Future Work

In this paper, we illustrated how physical- and control-layer subsystems of GFM IBRs with different primary controls can be represented as analog equivalent circuits. Through single-unit and network-scale simulations, we validated the concept. Computational effort involved was noted to be significantly reduced with the equivalent-circuit modeling paradigm and no loss in accuracy was observed. As part of future work, we will include other distinguishing attributes into GFM IBR models, e.g., current limiters and DC-side behavior, as well as pursue integrated equivalent-circuit modeling of machines, grid-following IBRs, and grid-forming IBRs.

Acknowledgements

This work was authored in part by the National Renewable Energy Laboratory (NREL), operated by Alliance for Sustainable Energy, LLC, for the U.S. Department of Energy (DOE) under Contract No. DE-AC36-08GO28308. This work was supported by the Laboratory Directed Research and Development (LDRD) Program at NREL and the U.S. Department of Energy Office of Energy Efficiency and Renewable Energy (EERE) under the Solar Energy Technologies Office Award Number 38637 (UNIFI consortium). Brian Johnson was also supported by NSF CAREER Award 2314415.

References

[1] J. D. Lara, R. Henriquez-Auba, D. Ramasubramanian, S. Dhople, D. S. Callaway, and S. Sanders, "Revisiting power systems time-domain simulation methods and models," *IEEE Transactions on Power Systems (to be published)*, pp. 1–16, 2023.

[2] Y. Lin, J. H. Eto, B. B. Johnson, J. D. Flicker, R. H. Lasseter, H. N. Villegas Pico, G.-S. Seo, B. J. Pierre, and A. Ellis, "Research roadmap on grid-forming inverters," National Renewable Energy Laboratory, Tech. Rep., 2020.

[3] P. Kundur, *Power system stability*. McGraw Hill, 2007.

[4] R. Middlebrook, "Modeling current-programmed buck and boost regulators," *IEEE Transactions on Power Electronics*, vol. 4, no. 1, pp. 36–52, 1989.

[5] C. T. Rim, D. Y. Hu, and G. H. Cho, "Transformers as equivalent circuits for switches: General proofs and dq transformation-based analyses," *IEEE Transactions on Industry Applications*, vol. 26, no. 4, pp. 777–785, 1990.

[6] M. K. Kazimierczuk and A. J. Edstrom, "Open-loop peak voltage feedforward control of pwm buck converter," *IEEE Transactions on Circuits and Systems I: Fundamental Theory and Applications*, vol. 47, no. 5, pp. 740–746, 2000.

[7] B. Johnson, M. Lu, V. Purba, and S. Dhople, "Circuit-equivalent models for current-controlled inverters," in *Proc. IEEE Workshop on Control and Modeling for Power Electronics*, 2019, pp. 1–5.

[8] M. Lu, V. Purba, S. V. Dhople, and B. B. Johnson, "Unified equivalent-circuit models for voltage-source inverters that capture averaged dynamics and power-flow solutions in distribution networks," in *Proc. Hawaii International Conference on System Sciences*, 2021, pp. 1–10.

[9] R. Billmeyer, M. Lu, B. Johnson, and S. Dhople, "Modeling and simulation of power-electronic inverters in analog electronic circuit simulators," in *Proc. IEEE International Symposium on Circuits and Systems*, 2021, pp. 1–5.

[10] B. B. Johnson, T. Roberts, O. Ajala, A. D. Domínguez-García, S. V. Dhople, D. Ramasubramanian, A. Tuohy, D. Divan, and B. Kroposki, "A generic primary-control model for grid-forming inverters: Towards interoperable operation & control," in *Proc. Hawaii International Conference on System Sciences*, 2022, pp. 1–10.

[11] D. Venkatramanan, M. K. Singh, O. Ajala, A. Domínguez-García, and S. Dhople, "Integrated system models for networks with generators & inverters," in *Bulk Power Systems Dynamics and Control Symposium*, 2022, pp. 1–19, available at: arXiv preprint arXiv:2203.08253.

[12] F. Dörfler and D. Groß, "Control of low-inertia power systems," *Annual Review of Control, Robotics, and Autonomous Systems*, vol. 6, no. 1, pp. 415–445, 2023.

[13] A. Yazdani and R. Iravani, *Voltage-sourced converters in power systems: modeling, control, and applications*. John Wiley & Sons, 2010.

[14] O. Ajala, M. Lu, B. Johnson, S. V. Dhople, and A. Domínguez-García, "Model reduction for inverters with current limiting and dispatchable virtual oscillator control," *IEEE Transactions on Energy Conversion*, vol. 37, no. 4, pp. 2250–2259, 2021.

[15] M. C. Chandorkar, D. M. Divan, and R. Adapa, "Control of parallel connected inverters in standalone ac supply systems," *IEEE Transactions on Industry Applications*, vol. 29, no. 1, pp. 136–143, 1993.

[16] S. D'Arco, J. A. Suul, and O. B. Fosso, "A virtual synchronous machine implementation for distributed control of power converters in smartgrids," *Electric Power Systems Research*, vol. 122, pp. 180–197, 2015.

[17] N. Baeckeland and G.-S. Seo, "Enhanced large-signal stability method for grid-forming inverters during current limiting," in *Proc. IEEE Workshop on Control and Modeling for Power Electronics*, 2023, pp. 1–8.